Journal of Materials Chemistry C

PAPER

View Article Online
View Journal | View Issue

Cite this: J. Mater. Chem. C, 2015, 3, 11645

Sandwich-structured Fe_2O_3@SiO_2@Au nanoparticles with magnetoplasmonic responses†

Zhongyu Cai,*[ab] Eunice S. P. Leong,[c] Zhigang Wang,[a] Wenxin Niu,[a] Weiqing Zhang,[a] Serge Ravaine,[d] Nikolai L. Yakovlev,[c] Yan Jun Liu,*[c] Jinghua Teng*[c] and Xianmao Lu*[a]

Received 5th May 2015,
Accepted 9th October 2015

DOI: 10.1039/c5tc01259g

www.rsc.org/MaterialsC

We report a method for the fabrication of relatively uniform sandwich-like core-interlayer-shell nanostructures by using γ-Fe_2O_3 as the inner core, SiO_2 as the interlayer, and relatively uniform gold (Au) as the outer shell. The resulting novel hybrid nanoparticle combines the intense local fields of nanorods with the highly tunable plasmon resonances of nanoshells. The length and diameter of the resulting nanoparticles can be tuned by the aspect ratio of α-Fe_2O_3, the interlayer of SiO_2 and the outer layer of Au. After calcination under H_2 and then exposure to air, α-Fe_2O_3 was transformed into γ-Fe_2O_3, which provides the hybrid particle magnetic tunability. This metal oxide (γ-Fe_2O_3) dielectric core, the SiO_2 interlayer and the Au shell spindle nanoparticle resemble a grain of Au nanorice (γ-Fe_2O_3@SiO_2@Au ellipsoids). The core-interlayer-shell geometry possesses greater structural and magnetic tunability than a nanorod or a nanoshell. The plasmon resonance of this novel γ-Fe_2O_3@SiO_2@Au geometry is believed to arise from a hybridization of the primitive plasmons of an ellipsoidal cavity inside a continuous Au shell. The unique magnetoplasmonic properties of this γ-Fe_2O_3@SiO_2@Au nanostructure are highly attractive for applications such as surface plasmon resonance sensing because of the dipole resonance of the resultant nanostructure and recyclable catalysts arising from the outer Au layer and the inner magnetic γ-Fe_2O_3 core.

1. Introduction

Core–shell nanostructures that combine the properties of both the core and shell materials have attracted intense research interest in recent years due to their potential for various applications in renewable energy, environmental cleanup, biomedicine, nanophotonics and energy storage.[1–12] In general, core–shell nanoparticles (NPs) can be classified into dielectric core@dielectric shell, metal core@dielectric shell, and metal core@metal shell structures.[13] The rapid development in plasmonics has intrigued much interest in novel dielectric core@metal shells because of the more flexibility in engineering their plasmonic properties. Plasmonic dielectric core@metal shell NPs have strong optical absorption and scattering properties, which can span a large region of the electromagnetic spectrum from visible to far-infrared.[14,15] The remarkable plasmonic properties of these types of NPs have led to numerous applications, from fluorescence enhancement of weak molecular emitters, substrates for surface plasmon resonance (SPR) sensing, biosensing, surface enhanced Raman and surface enhanced infrared absorption spectroscopy, to contrast enhancement in bioimaging and photothermal cancer therapy.[2–6,8,16]

The root of the remarkable plasmonic properties of these kinds of NPs is their geometry-dependent, plasmon-derived optical resonances whose frequencies depend sensitively on the inner and outer dimensions of their metallic shell layers. Various methods have been developed for the fabrication of dielectric core@metal shell NPs.[5] Halas and co-workers pioneered the fabrication of dielectric core@metal shell NPs.[6,14,17] In their method, the surface of the dielectric core was first functionalized with an organosilane derivative bearing an amine functional group. Then the core is attached with tiny gold (Au) NPs. Finally, a plating solution is used to grow Au layers on the core.[17] By using this method, relatively complete

[a] Department of Chemical and Biomolecular Engineering, National University of Singapore, 4 Engineering Drive 4, Singapore 117585. E-mail: chelxm@nus.edu.sg; Fax: +65-6779-1936; Tel: +65-6516-1071
[b] Department of Chemistry, University of Pittsburgh, Pittsburgh, Pennsylvania, 15260, USA. E-mail: chemczy@gmail.com; Tel: +1-412-624-6313
[c] Institute of Materials Research and Engineering, Agency for Science, Technology and Research (A*STAR), 3 Research Link, Singapore 117602. E-mail: jh-teng@imre.a-star.edu.sg, liuy@imre.a-star.edu.sg; Fax: + 65-6872-0785; Tel: +65-6874-8137, +65-6513-1358
[d] CNRS, Univ. Bordeaux, CRPP, UPR 8641, F-33600 Pessac, France

† Electronic supplementary information (ESI) available: SEM images of α-Fe_2O_3 NPs, summary of the average size and size distribution of α-Fe_2O_3 NPs, the XPS spectra of α-Fe_2O_3 NPs, TEM images of α-Fe_2O_3@Au NPs, SAED patterns of γ-Fe_2O_3@SiO_2, photographs of γ-Fe_2O_3@SiO_2@Au NP solution before and after adsorption and separation by a magnet and the transmission spectra of γ-Fe_2O_3@SiO_2@Au ellipsoids in a magnetic field with different angles along their longitudinal direction. See DOI: 10.1039/c5tc01259g

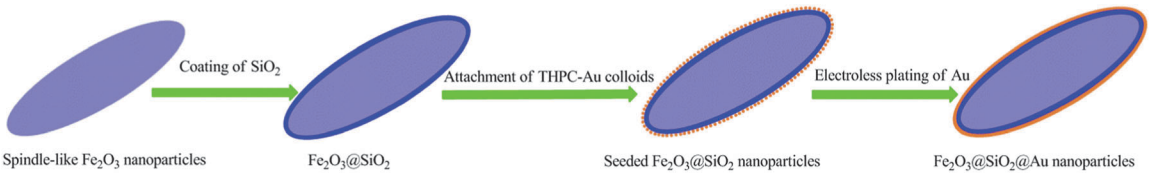

Scheme 1 Schematic illustration of hematite-SiO_2–Au core-interlayer-shell NPs.

Au shells can be fabricated. This method is feasible for the fabrication of dielectric core@Au shell NPs. Recently, some other investigators also tried to fabricate such a dielectric core@metal shell structure using different methods. Yu and co-authors reported the synthesis, characterization and properties of α-Fe_2O_3@SiO_2/Au NPs, in which hematite cubic α-Fe_2O_3 was firstly coated with one layer of SiO_2. The resulting spherical structure was then attached with Au NPs.[18] In another study, Peng *et al.* described the synthesis of spherical γ-Fe_2O_3/SiO_2/Au magnetic composites with sparse Au nanoparticles on the surface of the SiO_2 layer.[19] Liz-Marzán *et al.* and Ma *et al.* have demonstrated the fabrication of spindle-like α-Fe_2O_3@Au NPs, respectively, using a similar layer-by-layer assembly method in combination with the seed growth method.[20,21] A continuous Au shell has been fabricated through adsorption and subsequent metallization on Au-seeded APTES-grafted silica spheres. But the resulting Au shell is still very rough which leads to a broad plasmonic peak.[22] In spite of these studies, the fabrication of NPs with instantaneous and reversible tuning of the plasmonic properties remains a challenge. Furthermore, future development in this area requires these plasmonic NPs to possess a versatile structure and tunable electrical, optical or magnetic properties.[23–25]

Here we report a spindle-like hybrid nanostructure geometry that combines the plasmonic properties of both magnetic nanorods and noble metallic nanoshells in a single structure. Uniform sandwich-like core-interlayer-shell NPs are fabricated by using γ-Fe_2O_3 ellipsoids as the inner core, SiO_2 as the interlayer, and uniform Au as the outer shells (Scheme 1), which is different from the previously reported α-Fe_2O_3@Au nanostructure due to its magnetic core.[17,20,21] In this hybrid nanostructure, α-Fe_2O_3 ellipsoids with different aspect ratios were firstly synthesized by the precipitation of iron(III) perchlorate in the presence of urea. The ellipsoids were then modified with PVP and coated with SiO_2 *via* a modified Stöber method.[26–28] The core–shell NPs were reduced by H_2 and the ellipsoids became magnetic. Finally, the Au shell was grown on the surface of the γ-Fe_2O_3@SiO_2 NPs with different thicknesses by varying the amount of Au plating solution added. Such hybrid nanostructures possess both magnetic and plasmonic properties, indicating that they could be actively controlled by a magnetic field and hence are important for active plasmonics and recyclable catalysts.

2. Experimental section

2.1 Materials

Iron(III) perchlorate ($Fe(ClO_4)_3{\cdot}6H_2O$, Reagent Grade), sodium dihydrogen phosphate (NaH_2PO_4, Technical Grade), urea (NH_2CONH_2), poly(vinyl pyrrolidone) with an average molar mass of 360 kg mol^{-1} (PVP, K90), tetraethoxysilane (TEOS, 98%), tetramethylammonium hydroxide aqueous solution (TMAH, v/v, 10%), ethanol (≥99.7%), (3-aminopropyl) trimethoxysilane (APTMS, 97%), tetrachloroauric acid ($HAuCl_4{\cdot}3H_2O$), absolute ethanol, tetrakis hydroxymethyl phosphonium chloride (THPC) were purchased from Sigma-Aldrich. Chloroauric acid and potassium dihydrogen phosphate (KH_2PO_4) were obtained from Fisher Scientific (Hampton, NH). All the chemicals were used as received without further purification. Ultrapure water (18.2 MΩ resistivity) was obtained from a Milli-Q water purification system (Millipore, Billerica, MA). (**Caution!** Ethanol, CO, chloroauric acid, THPC, APTMS, APTES, and piranha present potential health and/or fire hazards. Appropriate precautions should be taken at all times.)

2.2 Preparation of γ-Fe_2O_3@SiO_2@Au NPs

Generally, there are four steps (Scheme 1) in the fabrication of γ-Fe_2O_3@SiO_2@Au NPs with tailored plasmon resonance: (1) synthesis of spindle-like α-Fe_2O_3; (2) coating of SiO_2 onto the surface of α-Fe_2O_3; (3) transformation of α-Fe_2O_3@SiO_2 into γ-Fe_2O_3@SiO_2 and attachment of colloidal Au NPs; (4) plating of Au onto the seeded γ-Fe_2O_3@SiO_2 NPs.

2.2.1 Preparation of α-Fe_2O_3 NPs. Uniform α-Fe_2O_3 ellipsoids with different aspect ratios were synthesized by precipitation of iron(III) perchlorate in the presence of urea.[29] Briefly, 4.62 g of $Fe(ClO_4)_3{\cdot}6H_2O$ together with 0.036 g of NaH_2PO_4 and 0.60 g of urea were dissolved in 100 mL of deionized water in a triangular flask under ultrasonication at room temperature. The solution was kept undisturbed in an oven for 24 h at 100 °C before it was cooled slowly to room temperature. Centrifugation was applied to the dispersion to purify the hematite spindles at 6000 rpm, 30 min for six times, until a transparent supernatant was obtained. By varying the ratio between $Fe(ClO_4)_3{\cdot}6H_2O$ and NaH_2PO_4, the aspect ratio of Fe_2O_3 ellipsoids can be precisely controlled.

2.2.2 Preparation of α-Fe_2O_3@SiO_2 and γ-Fe_2O_3@SiO_2 NPs. We modified the surface of hematite cores with PVP, followed by silica coating using the Stöber method *via* the hydrolysis of TEOS (98%).[30] Specifically, 1.2 g PVP K90 were added to the dispersion (containing 0.1 g α-Fe_2O_3) to keep the hematite spindle stable, followed by centrifugation (8000 rpm for 40 min) to remove the unabsorbed PVP molecules. Silica coating of the spindle hematite (0.1 g) was carried out in 100 mL of ethanol in the presence of 6 mL of water and 0.2 mL of TMAH (v/v 10%) as the base catalyst. 2 mL of TEOS were added to the system every 2 h for certain times to achieve different aspect ratios. Strong ultrasonication was applied during the coating process to prevent the spindles from crosslinking. The ellipsoids with a maghemite core were obtained by reducing the hematite core in H_2 at 360 °C for 4 h,

followed by exposure to the air at 240 °C for 2 h. After calcination, the ellipsoids were redispersed in ethanol under ultrasonication for 4 h.

2.2.3 Preparation of γ-Fe_2O_3@SiO_2@Au NPs. The seed particles (γ-Fe_2O_3@SiO_2@THPC-Au) used in the present study were fabricated following a similar procedure as the method for the immobilization of Au NPs on silica surfaces.[17] The surface of the spindle-shaped γ-Fe_2O_3@SiO_2 particles was functionalized with organosilane molecules (APTMS) to generate an amine moiety-coated surface. Typically, 600 μL of APTMS was introduced into 5 mL of ethanol solution of γ-Fe_2O_3@SiO_2 particles under vigorous stirring. The surface functionalization of γ-Fe_2O_3@SiO_2 particles was accomplished by stirring the mixture for 12 h. The resulting particles were centrifuged and redispersed in ethanol several times to remove the excess APTMS. THPC-capped Au NPs (~2 nm in diameter) were prepared following Duff's method,[31] and then attached to the functionalized γ-Fe_2O_3@SiO_2 particle surfaces through Au-amine interaction.[32] These attached Au colloids acted as the nucleation sites for the reduction of Au ions from solution onto the γ-Fe_2O_3@SiO_2 surface until continuous and complete Au nanoshells were formed.[14]

The γ-Fe_2O_3@SiO_2@Au NPs were fabricated *via* seed-catalyzed reduction of $AuCl_4^-$ ions by CO in aqueous solutions at room temperature. A 44 μM aqueous $HAuCl_4$ plating solution was prepared by the addition of 3 mL of 1 wt% $HAuCl_4$ to 200 mL of 1.8 mM aqueous K_2CO_3 and was stored for a minimum of 24 h before use. For a typical process, a certain amount of γ-Fe_2O_3@SiO_2@THPC-Au was added into a small glass vial containing 3 mL of $HAuCl_4$ plating solution. The growth of complete Au shells typically took 5 min. By adjusting the amount ratio between seed particles and $AuCl_4^-$ ions, the thickness of the Au shells can be precisely controlled. The resulting γ-Fe_2O_3@SiO_2@Au NPs can be homogenously dispersed in water to form colloidal solutions.

2.3 Characterization

Scanning electron microscope (SEM) images were obtained on a JEOL JSM-6700F field emission SEM (FESEM) at an acceleration voltage of 5.0 kV. The samples for SEM measurements were prepared by drying a drop of colloidal solutions on the silicon wafer surface. Transmission electron microscopy (TEM) and selected area electron diffraction (SAED) images were obtained using a JEOL JEM-2100F transmission electron microscope at an acceleration voltage of 200 kV. X-ray diffraction (XRD) patterns were recorded on a Shimadzu XRD-6000 X-ray diffractometer using Cu Kα as the irradiation source, operated at 40 kV and 30 mA. The magnetic properties of the samples were measured using a superconducting quantum interference device (SQUID) magnetometer under an in-plane applied magnetic field between −10 000 and 10 000 Oe at room temperature. The γ-Fe_2O_3@SiO_2@Au NPs with different geometries were dispersed into water to measure their transmission in solution. Then 3 mL of γ-Fe_2O_3@SiO_2@Au NP solution was put into a fused quartz cuvette with a path length of 1 cm. The transmission spectra were obtained using a Cary 5000 UV/Vis/NIR spectrophotometer in the wavelength range of 400−2400 nm. To investigate the angular effect of a magnetic field, the measurement of the optical transmission was performed by applying an external magnetic field with a surface magnetic strength of 3600 Gauss to the solutions. The probe was perpendicular to the glass vessel and parallel to the direction of the magnetic field. Compositional investigation for the samples was carried out using an X-ray photoelectron spectroscope (XPS, AXIS-HSi, Kratos Analytical). The X-ray photoelectron spectra of the studied elements were calibrated with the C1s peak arising from adventitious carbon with a binding energy of 284.6 eV.

2.4 Simulation

To understand the optical response of the Fe_2O_3@SiO_2@Au nanoparticle, we modelled a single Fe_2O_3@SiO_2@Au spindle as an ellipse with a longitudinal diameter of 340 nm and a transverse diameter of 54 nm. The thickness of the SiO_2 layer was set as 12 nm whereas the outer Au shell layer thickness was 16 nm. The n–k value of Fe_2O_3 is obtained from ref. 33. A fine mesh of 5 nm is applied to the structure. PML boundary conditions are applied in the x–y–z directions and both the scattering and absorption of light from the spindle are calculated to determine the extinction of light. As the measurement is carried out under unpolarized light, both the x and y polarizations are calculated to determine scattering using unpolarized light. It is found that scattering is mainly influenced by the x polarized light (*i.e.*, polarization along the longitudinal direction). The electric field and magnetic field distribution at the two peaks is also plotted for the x polarization.

3. Results and discussion

3.1 α-Fe_2O_3 NPs with different aspect ratios

Hematite spindles with different aspect ratios were synthesized by forced hydrolysis of iron salt. The sizes and shapes of the products were characterized by TEM. The aspect ratio (c/a) of spindles is defined as the ratio of the major axis length (c) to the minor axis width (a). The recipe is shown in Table 1. It has been reported that the molar ratio between Fe^{3+} and H_2PO^{4-} has a great influence on the aspect ratio of spindles.[29]

By decreasing the Fe^{3+}/H_2PO^{4-} molar ratio from 33.3 to 13.3, the aspect ratio of spindles can be increased as indicated in Fig. 1a–c. Moreover, as shown in Fig. 1a–c and summarized in Table S1 (ESI†), large quantities of uniform spindles with narrow size distribution (<10%) were obtained, which also can be confirmed from the SEM image (Fig. S1, ESI†). Further investigation of the crystalline information of the hematite spindles was carried out using a high resolution TEM (HRTEM), as shown in Fig. 1d, which verified the hematite spindles to be single crystals with a rhombohedral phase as reported in the literature.[29]

Table 1 The experimental recipes for the preparation of hematite spindles at 100 °C for 24 h

Sample	Aspect ratio	Fe^{3+}/H_2PO^{4-}	$Fe(ClO_4)_3{\cdot}6H_2O$ (g L^{-1})	NaH_2PO_4 (g L^{-1})	Urea (g L^{-1})
1	9 : 1	13.3	46.2	0.900	6.0
2	6 : 1	18.4	46.2	0.650	6.0
3	4 : 1	23.1	46.2	0.520	6.0
4	3 : 1	33.3	46.2	0.360	6.0

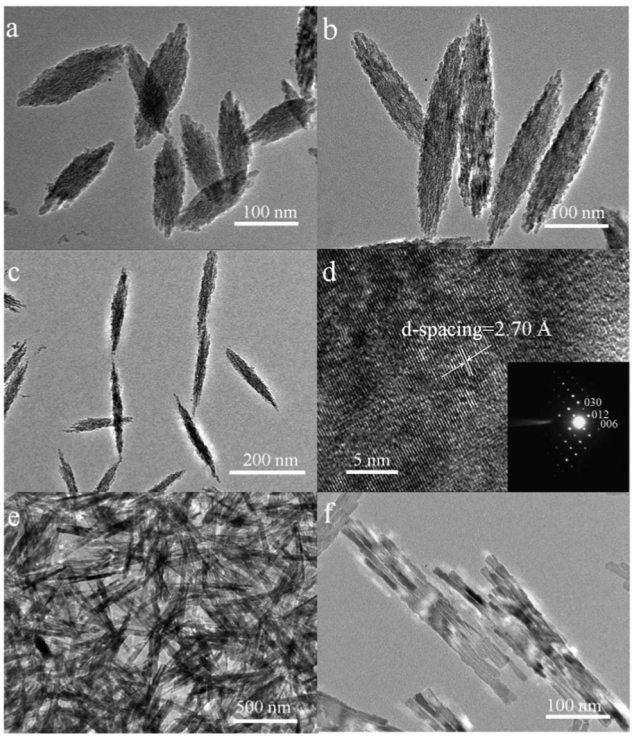

Fig. 1 TEM images of α-Fe_2O_3 NPs with aspect ratios of (a) 3, (b) 6, and (c) 9; (d) HRTEM of the α-Fe_2O_3 NPs (the inset shows the SAED pattern of the hematite spindles); (e and f) α-Fe_2O_3 NPs with an aspect ratio larger than 12.

The *d*-spacing of the lattice 0.27 nm, corresponds to the (104) face of α-Fe_2O_3. The inset SAED pattern of Fig. 1d further confirms the single crystalline of α-Fe_2O_3 with the rhombohedral phase. It should be mentioned that further decrease of the Fe^{3+}/H_2PO^{4-} molar ratio to 12 leads to the formation of bamboo-like hematite with a relatively large aspect ratio (Fig. 1e and f). To our best knowledge, this is the first finding in the synthesis of α-Fe_2O_3. The investigation of the mechanism is in progress.

3.2 α-Fe_2O_3@SiO_2 and γ-Fe_2O_3@SiO_2 NPs

The most frequently used coupling agent for coating colloidal particles with one layer of SiO_2 is PVP.[34] It is believed that PVP molecules behave not only as an absorbent of TEOS, but also as a surface stabilizer of spindles. It is well known that SiO_2 coating offers possibilities for the shape control of a particle. The smooth SiO_2 surface enables the advantage of coating a smooth Au shell. The silica coating procedure is in fact a process of hydrolysis of TEOS on the surface of spindle cores in the manner of layer-by-layer.[27,35] To avoid the self-nucleation of the silica spheres, the amount of TEOS needs to be precisely controlled in each addition.[26]

Fig. 2 shows the TEM images of α-Fe_2O_3@SiO_2 ellipsoids with different aspect ratios and SiO_2 shell thicknesses. As shown in Fig. 2a, upon coating with SiO_2, the rough surface of α-Fe_2O_3 becomes a smooth SiO_2 surface of α-Fe_2O_3@SiO_2 ellipsoids. The thickness of the SiO_2 layer can be easily tuned by varying the amount of TEOS added into the α-Fe_2O_3 solution. Thick SiO_2 coating can be achieved by repeating the addition of

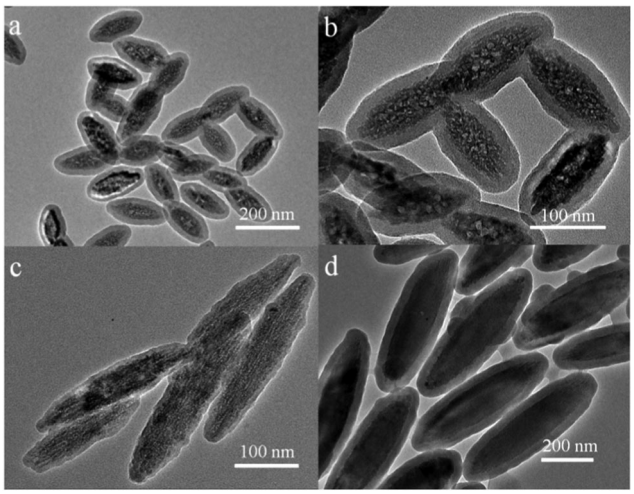

Fig. 2 TEM images of the fabricated α-Fe_2O_3@SiO_2. (a) α-Fe_2O_3@SiO_2 at low magnification (aspect ratio of 3); (b) α-Fe_2O_3@SiO_2 (aspect ratio of 3) with an average shell thickness of 22.6 nm; (c) α-Fe_2O_3@SiO_2 (aspect ratio of 6) with an average shell thickness of 11.8 nm; (d) α-Fe_2O_3@SiO_2 (aspect ratio of 6) with an average shell thickness of 33.5 nm.

TEOS. It is found that the shell thickness is ~23 nm when adding 50 μL of TEOS into a solution containing 0.05 g of α-Fe_2O_3. As shown in Fig. 2b, the aspect ratio of the resulting α-Fe_2O_3@SiO_2 drops from ~3 for bare hematite spindle cores to ~2 upon increasing the amount of TEOS. Fig. 2c and d clearly demonstrate the core–shell architecture of the synthesized ellipsoids with an aspect ratio of 6. As shown in the TEM images, the thickness of the silica shell varied from 11 to 33 nm for different samples after several cycles of SiO_2 coating. Comparing the lengths and widths of spindles after each cycle of SiO_2 coating, it is found that the size increase leads to a uniform coating of SiO_2 on α-Fe_2O_3 NPs. In addition, the polydispersities in both length and width decrease with the increasing amount of added TEOS. After adding a certain amount of TEOS, the polydispersity decreases below 5% as shown in Fig. 2, which is considered as the size polydispersity of individual unit cell building blocks in three-dimensional photonic crystals. Thus, these relatively monodisperse NPs may also find applications in photonic crystals.[24,27,36]

The XRD patterns of α-Fe_2O_3@SiO_2 and γ-Fe_2O_3@SiO_2 NPs are shown in Fig. 3. Characteristic diffraction peaks corresponding to α-Fe_2O_3 (012), (104), (110), (113), (024), (116), (018), (214), (300), (1010), (220) reflections can be found at 2θ = 24.149, 33.161, 35.629, 40.862, 49.463, 54.073, 57.607, 62.436, 63.998, 71.960, 75.451, respectively. In addition, the XRD pattern of the hematite spindle is also indexed to a rhombohedral phase (JCPDS No. 86-0550) and no other impurities such as FeOOH, γ-Fe_2O_3 and Fe_3O_4 can be seen here. After calcination in H_2 and then exposure to air, the α-Fe_2O_3@SiO_2 ellipsoids were transformed into γ-Fe_2O_3@SiO_2 ellipsoids as confirmed by the XRD pattern. The XRD pattern of γ-Fe_2O_3@SiO_2 NPs is also demonstrated in Fig. 3, matching γ-Fe_2O_3 well from standard JCPDS data (39-1346). Characteristic diffraction peaks corresponding to (220), (311), (400), (422), (511), (440), (533) reflections can be

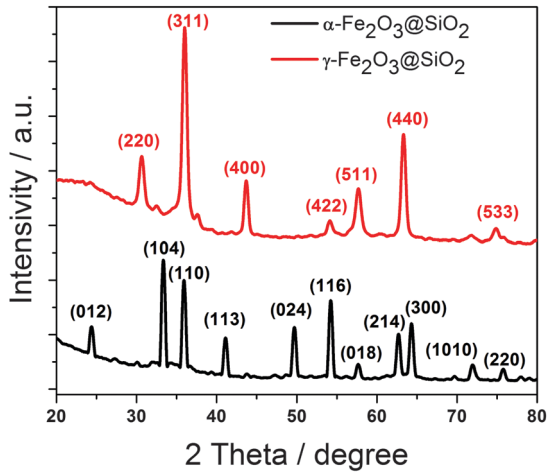

Fig. 3 XRD patterns of the α-Fe_2O_3@SiO_2 and γ-Fe_2O_3@SiO_2 powder with an aspect ratio of 3.

found at 2θ = 30.241, 35.630, 43.84, 53.733, 57.271, 62.925, 71.820, 74.471, respectively. The XPS spectra of α-Fe_2O_3@SiO_2 NPs were also recorded as shown in Fig. S2 (ESI†). It shows that the coating of SiO_2 leads to low Fe_2O_3 peak intensity.

3.3 Fabrication of γ-Fe_2O_3@SiO_2@Au NPs

Fig. 4 shows TEM images of THPC-Au and γ-Fe_2O_3@SiO_2@THPC-Au. Fig. 4a shows that THPC-Au nanoparticles are rather uniform in size with a mean diameter of ~3 nm, which is consistent with the previous report.[31] Fig. 4b shows a low magnification TEM image of γ-Fe_2O_3@SiO_2 covered with THPC Au NPs. The SAED pattern of the samples confirms that the spindles are γ-Fe_2O_3 instead of α-Fe_2O_3 as shown in Fig. S3 (ESI†). This is consistent with the XRD results and the data reported by Guivar *et al.*[37] Fig. 4c and d show HRTEM of γ-Fe_2O_3@SiO_2 NPs covered with THPC Au NPs. As can be seen, THPC Au NPs are uniformly distributed on the surface of γ-Fe_2O_3@SiO_2. This uniform distribution of THPC Au NPs may facilitate the growth of relatively smooth and complete Au shells. The clear crystalline structure with a *d*-spacing of ~2.36 Å corresponds to the 111 plane of Au (Fig. 4d).

Fig. 5 shows the γ-Fe_2O_3@SiO_2@Au NPs fabricated using the seed growth method. By varying the amount of $HAuCl_4$ used in the seed growth process, the shell thickness of the Au outer layer can be precisely tuned. The Au shell thickness increases with the amount of Au plating solution (Fig. 5a–c). And the shell becomes from incomplete (Fig. 5a) to complete (Fig. 5b). Fig. 5d shows the γ-Fe_2O_3@SiO_2@Au NPs with an aspect ratio of 6 at low resolution. This indicates that the present method is effective since all the NPs were coated with a continuous Au layer. The high-resolution image (Fig. 5f) shows that a relatively good quality of Au shell can be obtained even with a less amount of plating solution. The energy dispersive X-ray (EDX) image of the γ-Fe_2O_3@SiO_2@Au ellipsoids indicate that the Au NPs were grown onto the surface of γ-Fe_2O_3@SiO_2 (Fig. 5g and h). In this study, by changing the amount of Au plating solution, the shell thickness of Au can be tuned from ~11.5 nm to ~15.5 nm. The adjustable Au thickness can be used to tune the spectra of the

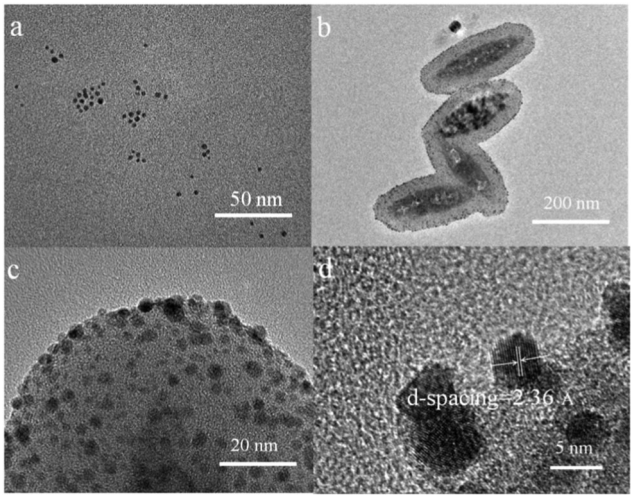

Fig. 4 TEM images of (a) THPC Au; (b) γ-Fe_2O_3@SiO_2 attached with THPC Au; (c) distribution of THPC Au onto γ-Fe_2O_3@SiO_2; (d) HRTEM of THPC Au attached onto γ-Fe_2O_3@SiO_2.

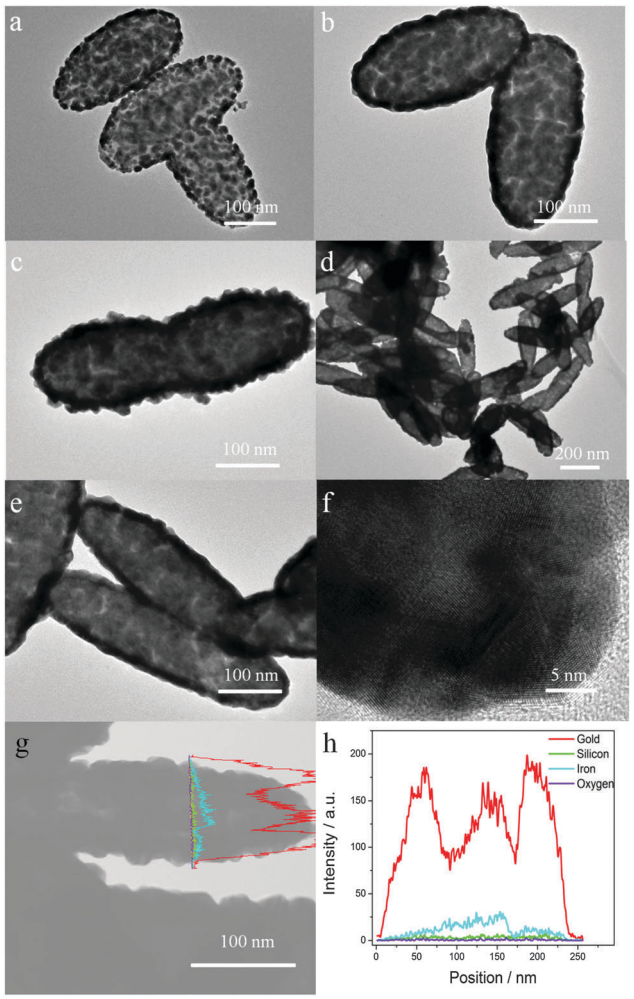

Fig. 5 TEM images of γ-Fe_2O_3@SiO_2@Au NPs (aspect ratio of 3) fabricated with (a) 10 μL, (b) 20 μL, and (c) 30 μL of Au plating solution; (d–f) γ-Fe_2O_3@SiO_2@Au NPs (aspect ratio of 6) fabricated with 20 μL Au plating solution at different magnifications; (g) and (h) EDX of the γ-Fe_2O_3@SiO_2@Au ellipsoids.

resulting core–shell structure. The relatively smooth and complete Au layers can be attributed to many factors, especially the SiO_2 interlayer. Comparing to the samples fabricated without the SiO_2 layer, the γ-Fe_2O_3@SiO_2@Au ellipsoids are much smoother (Fig. S4, ESI†). Fig. S3 (ESI†) shows the morphology of Fe_2O_3@Au ellipsoids with different aspect ratios fabricated under the same conditions as that of γ-Fe_2O_3@SiO_2@Au ellipsoids. The resulting Fe_2O_3@Au ellipsoids have a relatively rough sea cucumber-like surface. Therefore, the SiO_2 layer on the surface of γ-Fe_2O_3 not only prevents the as-reduced magnetic γ-Fe_2O_3 from aggregation but also facilitates the surface functionalization of ellipsoids with amino-groups for linking to THPC Au NPs. It should also be pointed out that the current method using CO reduction of Au is advantageous over other methods since the resulting Au shell is relatively complete and smooth.[17,20,21,38,39]

Fig. 6 shows the magnetization (M–H) curves of both α-Fe_2O_3@SiO_2@Au and γ-Fe_2O_3@SiO_2@Au ellipsoids measured using a SQUID at room temperature. It clearly shows that the γ-Fe_2O_3@SiO_2@Au ellipsoids have relatively strong ferromagnetic properties while the α-Fe_2O_3@SiO_2@Au NPs only have very weak ones, which indicates that the γ-Fe_2O_3@SiO_2@Au ellipsoids can be actively controlled by the external magnetic field and will be potentially useful for a wide range of applications. The saturation magnetization of γ-Fe_2O_3@SiO_2@Au NPs was estimated to be 17 emu g^{-1}. The photographs of γ-Fe_2O_3@SiO_2@Au NP solution before and after adsorption and separation by a magnet were obtained to further confirm the magnetic properties of γ-Fe_2O_3@SiO_2@Au NPs. As shown in Fig. S5 (ESI†), the clear solution was obtained after the separation by a magnet, indicating the magnetic properties of γ-Fe_2O_3@SiO_2@Au NPs.

The γ-Fe_2O_3@SiO_2@Au ellipsoids prepared in this study is a novel structure with unique magnetoplasmonic properties that have never been reported before. Yu and co-authors described the synthesis, characterization and properties of α-Fe_2O_3@SiO_2/Au NPs.[18] Peng *et al.* demonstrated the synthesis of spherical γ-Fe_2O_3/SiO_2/Au magnetic composites with sparse Au nanoparticles on the surface of the SiO_2 layer.[40] Both studies demonstrated the fabrication of spherical NPs attached with Au NPs while ours are spindle shaped. In addition, there was no continuous Au shell formed in both cases. As mentioned earlier, the spindle structure of our γ-Fe_2O_3@SiO_2@Au NPs combines the plasmonic properties of both magnetic nanorods and nanoshells in a single structure.[19] This spindle geometry possesses greater structural tunability than a nanorod or a spherical nanoshell. Therefore, none of the above two studies is identical with the present study. Liz-Marzán *et al.* and Ma *et al.* have reported the fabrication of spindle-like α-Fe_2O_3@Au NPs, respectively.[20,21] However, the Au shell is very rough and the optical properties are less tunable. In addition, the resulting α-Fe_2O_3@Au NPs lack the unique magnetoplasmonic properties.

3.4 Optical properties of γ-Fe_2O_3@SiO_2@Au NPs

Fig. 7 shows the UV-vis-NIR transmission of γ-Fe_2O_3@SiO_2@Au with different aspect ratios and Au shell thicknesses. The γ-Fe_2O_3@SiO_2@Au NP with an aspect ratio of 6 shows two peaks. The peaks at longer and shorter wavelengths correspond to the longitudinal and transverse modes of the surface plasmons of γ-Fe_2O_3@SiO_2@Au ellipsoids, respectively. The peak wavelengths of transverse modes red-shift from 500 to 550 nm when the shell thickness of Au increases for a fixed aspect ratio of 6, while they blue shift for an aspect ratio of 3. This is because the transverse mode also greatly depends on the dielectric properties of the surrounding media and absorption cross section of the NP. From Fig. 7, one can observe that for a fixed aspect ratio, the transverse mode of the γ-Fe_2O_3@SiO_2@Au ellipsoids shows a clear trend, while for different aspect ratios, they may demonstrate either a blue shift or a red shift. Given that the surrounding media of the Au nanoshell can be considered the same for all the NPs, we mainly attribute this difference to the different absorption cross sections of the NPs. The broad longitudinal plasmons remain at the same position when the shell thickness increases from 11.5 nm to 15.5 nm. The strong plasmon resonance feature observed in the spectra in Fig. 7 arises from the longitudinal plasmon of this layered structure and exhibits a highly sensitive structural dependence of its optical resonance, which blue shifts as the metal layer thickness is increased. The γ-Fe_2O_3@SiO_2@Au NPs possess both

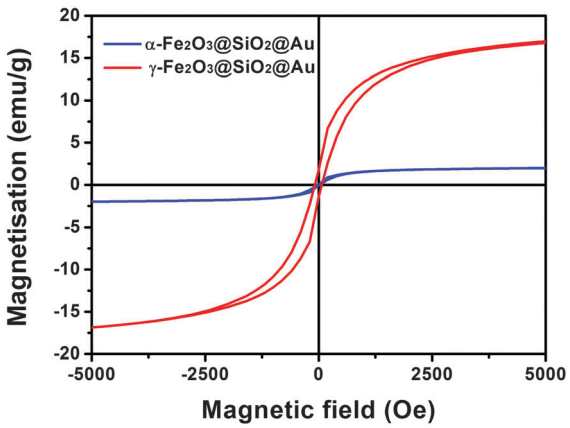

Fig. 6 Magnetic hysteresis loops of α-Fe_2O_3@SiO_2@Au and γ-Fe_2O_3@SiO_2@Au NPs.

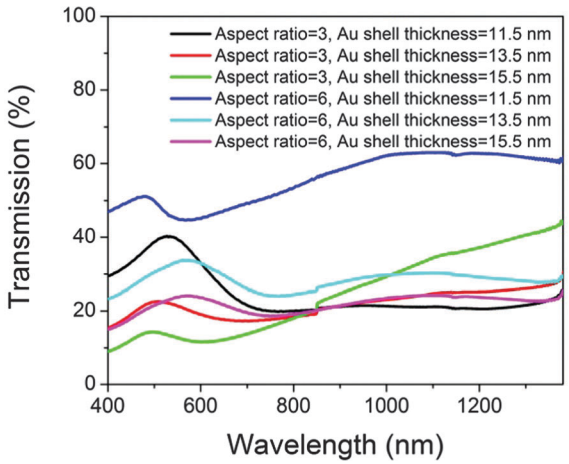

Fig. 7 Measured transmission spectra of γ-Fe_2O_3@SiO_2@Au ellipsoids with different aspect ratios and Au shell thicknesses.

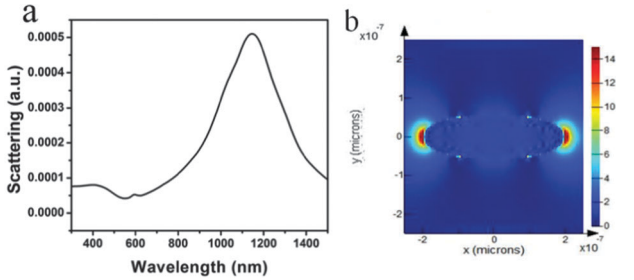

Fig. 8 (a) Calculated far-field extinction spectrum of the γ-Fe_2O_3@SiO_2@Au ellipsoids with incident polarization along the longitudinal axis of a nanorice particle using FDTD. The γ-Fe_2O_3@SiO_2@Au ellipsoids employed for the FDTD simulations is composed of a hematite core with a longitudinal diameter of 340 nm and a transverse diameter of 54 nm surrounded by a 16 nm-thick Au shell. (b) Near-field profile of the γ-Fe_2O_3@SiO_2@Au ellipsoids under resonance excitation (λ_{ex} = 1148 nm) with the incident polarization along the longitudinal axis.

magnetic and plasmonic properties, indicating that they could be actively controlled by a magnetic field and hence are important for active plasmonics.[41–43] Fig. S6 (ESI†) shows the tunable SPR bands under a magnetic field at different angles. The unique magneto-plasmonic properties of such γ-Fe_2O_3@SiO_2@Au NPs are extremely attractive for SPR sensing as a result of the dipole resonance of the novel nanostructure and recyclable catalysts arising from the outer layer Au shell and the magnetic core.[44,45]

The transmission of γ-Fe_2O_3@SiO_2@Au NPs is similar to the study conducted by Halas and coworkers except for the broad longitudinal plasmons.[46] It should be pointed out that the samples are measured under different conditions. We measured the transmission spectra of γ-Fe_2O_3@SiO_2@Au ellipsoid samples that dispersed in H_2O using a UV/Vis/NIR spectrophotometer, whereas in their study, they measured the extinction spectra of monolayers of α-Fe_2O_3@ @Au isolated nanoshells immobilized on PVP-glass slides using a dark field microscope.

We also simulated the optical response of the core–shell structures. A finite difference time domain (FDTD) analysis of the far field scattering spectrum of such a nanostructure reveals that the transverse mode has a much weaker scattering cross section than the longitudinal plasmon mode (Fig. 8).[47] In addition, the measured transmission in our experiment could be mainly attributed to the forward scattering of the γ-Fe_2O_3@SiO_2@Au NPs. From this point of view, the simulated results are in reasonable agreement with the measurements. The difference between the measurement and simulation might be mainly attributed to the shape tolerance and refractive index differences. The refractive index of γ-Fe_2O_3 was derived by fitting the experimental data in a previous report.[33]

4. Conclusions

Uniform ellipsoidal α-Fe_2O_3-core@SiO_2-interlayer NPs were fabricated by repeating silica coating on the surface of PVP modified hematite spindle cores. By repeating hydrolysis of TEOS, we can obtain ellipsoids with a low aspect ratio (<2). Due to the mechanism of hydrolysis of TEOS, polydispersity decreases upon increasing the amount of TEOS. These uniform ellipsoids with hematite cores can be transformed into magnetic ones (γ-Fe_2O_3@SiO_2) *via* calcination in H_2 and then exposure to air. γ-Fe_2O_3@SiO_2@Au NPs were further fabricated *via* a seed growth method and characterized using a UV-Vis spectrophotometer. It is found that γ-Fe_2O_3@SiO_2@Au NPs with large aspect ratios show two peaks. However, for low aspect ratios, there is only one plasmonic resonance peak. In addition, the magnetic γ-Fe_2O_3@SiO_2@Au NPs could show tailored SPR under a magnetic field, which is useful for fabricating tunable optical nanostructures.[25] The unique magnetoplasmonic properties of this new nanostructure are highly attractive for applications such as SPR sensing because of the dipole resonance of the resultant nanostructure and recyclable catalysts arising from the outer layer Au shell and the magnetic core.

Acknowledgements

The authors thank D. B. Zhou, Z. Q. Li, and Professor. H. T. Dai from Tianjin University to measure the magnetic hysteresis loop of the samples using a SQUID. Zhongyu Cai acknowledges a graduate scholarship from the National University of Singapore. We thank for the kind help from Professor. Saif Khan and Mr Prasanna Ganesan K. This work was supported by the joint French-Singaporean MERLION program under Grant No. R-279-000-334-133 and Agency for Science, Technology and Research (A*STAR) under Grant No. 0921540099 and 0921540098.

Notes and references

1 A. O. Govorov and H. H. Richardson, *Nano Today*, 2007, **2**, 30–38.
2 N. J. Halas, S. Lal, W.-S. Chang, S. Link and P. Nordlander, *Chem. Rev.*, 2011, **111**, 3913–3961.
3 V. Giannini, A. I. Fernández-Domínguez, S. C. Heck and S. A. Maier, *Chem. Rev.*, 2011, **111**, 3888–3912.
4 M. B. Cortie and A. M. McDonagh, *Chem. Rev.*, 2011, **111**, 3713–3735.
5 S. Lal, N. K. Grady, J. Kundu, C. S. Levin, J. B. Lassiter and N. J. Halas, *Chem. Soc. Rev.*, 2008, **37**, 898–911.
6 R. Bardhan, S. Lal, A. Joshi and N. J. Halas, *Acc. Chem. Res.*, 2011, **44**, 936–946.
7 H. Wang, L. Chen, Y. Feng and H. Chen, *Acc. Chem. Res.*, 2013, **46**, 1636–1646.
8 P. K. Jain, I. H. El-Sayed and M. A. El-Sayed, *Nano Today*, 2007, **2**, 18–29.
9 Y. B. Zheng, B. Kiraly, P. S. Weiss and T. J. Huang, *Nanomedicine*, 2012, **7**, 751–770.
10 J. S. Chen, C. M. Li, W. W. Zhou, Q. Y. Yan, L. A. Archer and X. W. Lou, *Nanoscale*, 2009, **1**, 280–285.
11 Z. Wang, D. Luan, S. Madhavi, Y. Hu and X. W. Lou, *Energy Environ. Sci.*, 2012, **5**, 5252–5256.
12 Z. Cai, Z. Xiong, X. Lu and J. Teng, *J. Mater. Chem. A*, 2014, **2**, 545–553.
13 R. Ghosh Chaudhuri and S. Paria, *Chem. Rev.*, 2011, **112**, 2373–2433.

14 S. J. Oldenburg, R. D. Averitt, S. L. Westcott and N. J. Halas, *Chem. Phys. Lett.*, 1998, **288**, 243–247.
15 H. Wang, D. W. Brandl, F. Le, P. Nordlander and N. J. Halas, *Nano Lett.*, 2006, **6**, 827–832.
16 B. Sepúlveda, P. C. Angelomé, L. M. Lechuga and L. M. Liz-Marzán, *Nano Today*, 2009, **4**, 244–251.
17 B. E. Brinson, J. B. Lassiter, C. S. Levin, R. Bardhan, N. Mirin and N. J. Halas, *Langmuir*, 2008, **24**, 14166–14171.
18 F. Chun-Liu, Q. Kun, Z. Jianhua, W. Shangbin, L. Xiaoxuan and Y. Shu-Hong, *Nanotechnology*, 2008, **19**, 125601.
19 Z. Li, M. Peng, Y. Jin, X. Wang, Y. Cui and C. Chen, *Chin. Sci. Bull.*, 2011, **56**, 2911–2915.
20 M. Spuch-Calvar, J. Pérez-Juste and L. M. Liz-Marzán, *J. Colloid Interface Sci.*, 2007, **310**, 297–301.
21 Z. Ma, H. Han, S. Tu and J. Xue, *Colloids Surf., A*, 2009, **334**, 142–146.
22 N. Phonthammachai, J. C. Y. Kah, G. Jun, C. J. R. Sheppard, M. C. Olivo, S. G. Mhaisalkar and T. J. White, *Langmuir*, 2008, **24**, 5109–5112.
23 R. Bardhan, O. Neumann, N. Mirin, H. Wang and N. J. Halas, *ACS Nano*, 2009, **3**, 266–272.
24 Z. Cai, Y. J. Liu, X. Lu and J. Teng, *J. Phys. Chem. C*, 2013, **117**, 9440–9445.
25 M. Wang, C. Gao, L. He, Q. Lu, J. Zhang, C. Tang, S. Zorba and Y. Yin, *J. Am. Chem. Soc.*, 2013, **135**, 15302–15305.
26 H. Giesche, *J. Eur. Ceram. Soc.*, 1994, **14**, 205–214.
27 Z. Cai, J. Teng, D. Xia and X. S. Zhao, *J. Phys. Chem. C*, 2011, **115**, 9970–9976.
28 Z. Cai, Y. J. Liu, X. Lu and J. Teng, *ACS Appl. Mater. Interfaces*, 2014, **6**, 10265–10273.
29 M. Ocaña, M. P. Morales and C. J. Serna, *J. Colloid Interface Sci.*, 1999, **212**, 317–323.
30 T. Ding, K. Song, K. Clays and C.-H. Tung, *Adv. Mater.*, 2009, **21**, 1936–1940.
31 D. G. Duff, A. Baiker and P. P. Edwards, *Langmuir*, 1993, **9**, 2301–2309.
32 S. L. Westcott, S. J. Oldenburg, T. R. Lee and N. J. Halas, *Langmuir*, 1998, **14**, 5396–5401.
33 M. Gartner, M. Crisan, A. Jitianu, R. Scurtu, R. Gavrila, I. Oprea and M. Zaharescu, *J. Sol–Gel Sci. Technol.*, 2003, **26**, 745–748.
34 C. Graf, D. L. J. Vossen, A. Imhof and A. van Blaaderen, *Langmuir*, 2003, **19**, 6693–6700.
35 Z. Cai, J. Teng, Q. Yan and X. S. Zhao, *Colloids Surf., A*, 2012, **402**, 37–44.
36 Z. Cai, Y. J. Liu, E. S. P. Leong, J. Teng and X. Lu, *J. Mater. Chem.*, 2012, **22**, 24668–24675.
37 J. Guivar, A. Martínez, A. Anaya, L. Valladares, L. Félix and A. Dominguez, *Adv. Nanopart.*, 2014, **3**, 114–121.
38 N. Phonthammachai, J. C. Y. Kah, G. Jun, C. J. R. Sheppard, M. C. Olivo, S. G. Mhaisalkar and T. J. White, *Langmuir*, 2008, **24**, 5109–5112.
39 X. Xu and M. B. Cortie, *J. Phys. Chem. C*, 2007, **111**, 18135–18142.
40 Z. X. Li, M. L. Peng, Y. Y. Jin, X. F. Wang, Y. L. Cui and C. Chen, *Chin. Sci. Bull.*, 2011, **56**, 2911–2915.
41 V. K. S. Hsiao, Y. B. Zheng, B. K. Juluri and T. J. Huang, *Adv. Mater.*, 2008, **20**, 3528–3532.
42 G. Armelles, A. Cebollada, A. García-Martín and M. U. González, *Adv. Opt. Mater.*, 2013, **1**, 10–35.
43 G. Y. Si, Y. H. Zhao, E. S. P. Leong and Y. J. Liu, *Materials*, 2014, **7**, 1296–1317.
44 J. Homola, *Chem. Rev.*, 2008, **108**, 462–493.
45 X. Zhang, Y. L. Chen, R.-S. Liu and D. P. Tsai, *Rep. Prog. Phys.*, 2013, **76**, 46401–46441.
46 H. Wang, D. W. Brandl, F. Le, P. Nordlander and N. J. Halas, *Nano Lett.*, 2006, **6**, 827–832.
47 C. Oubre and P. Nordlander, *J. Phys. Chem. B*, 2004, **108**, 17740–17747.

